Since January 2020 Elsevier has created a COVID-19 resource centre with free information in English and Mandarin on the novel coronavirus COVID-19. The COVID-19 resource centre is hosted on Elsevier Connect, the company's public news and information website.

Chemical Data Collections 28 (2020) 100470

Contents lists available at ScienceDirect

Chemical Data Collections

journal homepage: www.elsevier.com/locate/cdc

Data Article

Azaphenantherene derivatives as inhibitor of SARS CoV-2 M^{pro}: Synthesis, physicochemical, quantum chemical and molecular docking analysis

M. Venkateshan[a], J. Suresh[a,*], M. Muthu[b], R. Ranjith Kumar[b]

[a] Department of Physics, The Madura College, Madurai – 625011, Tamilnadu, India
[b] Department of Organic Chemistry, Madurai Kamaraj University, Madurai-625021, Tamilnadu, India

ARTICLE INFO

Article history:
Received 27 April 2020
Revised 23 June 2020
Accepted 23 June 2020
Available online 25 June 2020

Keywords:
SARS Coronavirus
main protease
Azaphenantherene
QTAIM
Hirshfeld surface analysis

ABSTRACT

The crystal structure of 2-(1H-indol-3-yl)-4-phenyl-5,6-dihydrobenzo[h]quinoline-3-carbonitrile (Ia) and 2-(5-bromo-1H-indol-3-yl)-4-(4-methoxyphenyl)-5,6-dihydrobenzo[h]quinoline-3-carbonitrile (Ib) were elucidated using single crystal X-ray diffraction. The cyclohexadiene ring adopts screw boat conformation in compound (Ia) and distorted screw boat in compound (Ib). The pyridine ring is effectively planar. The qualitative and quantitative analyses of hydrogen bonding interactions in the compounds were done using Hirshfeld surface analysis, QTAIM and NCI. DFT/B3LYP level of theory was used to optimize both the compounds. These compounds drug-like behaviors were studied using HOMO-LUMO analysis. The molecular docking analysis against M^{pro} was carried out for the synthesized compounds and some suggested drugs for COVID-19. The docking results were then analyzed.

Specifications table

Subject area	*Organic Chemistry, Spectroscopy, Crystallography, DFT, Molecular docking*
Compounds	2-(1H-indol-3-yl)-4-phenyl-5,6-dihydrobenzo[h]quinoline-3-carbonitrile (Ia)2-(5-bromo-1H-indol-3-yl)-4-(4-methoxyphenyl)-5,6-dihydrobenzo[h]quinoline-3-carbonitrile (Ib)
Data category	*Crystallographic data*
Data acquisition format	*CIF for crystallography*
Data type	*Analyzed*
Procedure	*The title compound was characterized by spectral studies, single crystal X- ray diffraction, Hirshfeld surface, DFT, QTAIM, NCI and molecular docking studies.*
Data accessibility	**CCDC 1999442 (Ia)** and **CCDC 1999443 (Ib)** www.ccdc.cam.ac.uk/structures

1. Rationale

Azaphenantherene (Fig. 1) is a heterocyclic compound containing quinoline moiety. There are many quinoline derived drug candidates are best selling drugs in the market. They are advised for treating various medical conditions. The most

* Corresponding author.
E-mail address: principal@maduracollege.edu.in (J. Suresh).

https://doi.org/10.1016/j.cdc.2020.100470
2405-8300/

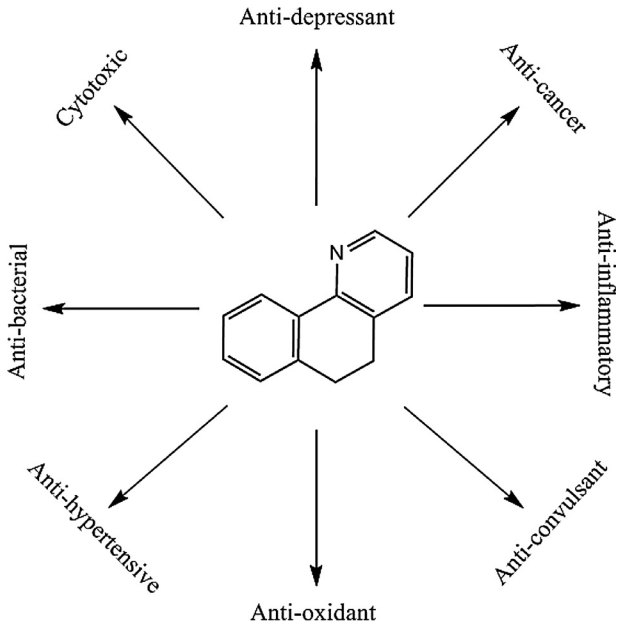

Fig. 1. Medicinal properties of azaphenantherene

promising property of quinoline derivatives is anti-malarial property. *Mefloquine* is a drug used to treat malaria [1]. *Parasite Vivax, P. malariae, P. falciparum* can be treated by *chloroquine* [2]. Bisquinoline, ferrocholoroquine and choloroquinolinylthiourea are found to possess good anti-malarial property [3,4]. Abadi and co-workers have found the analgesic property of fluoromethylquinoline [5]. The in-vitro and in-vivo studies showed some dihydroquinoline with the inhibition property against farnesyltransferase which can control the cell proliferation in breast cancer cell assay [6].

An epidermal growth factor receptor inhibitor *Pelitinib* and *Pyrotinib* are under clinical trial for lung cancer [7]. Some hydroxyquinolines [8] and anilinoquinolines [9] are screened for their anti-tumor properties.

The derivatives of methoxyquinolines showed anti-bacterial activity against Mycobacterium tuberculosis [10]. Anti-fungal activities of tetrahydroquinolines were evaluated against *Candida albicans* and it showed good anti-fungal property [11]. Massari and co-workers synthesized and screened some desfluoroquinolines against its anti-HIV [12].

Azaphenantherene is a pharmacologically active scaffold having cytotoxic [13] and anti-inflammatory [14] properties. Further, this can act as an agonist for serotonin 5HT receptor which is helpful as anti-depressant agent [15]. Recently, benzo[h]quinoline derivatives showed anti-bacterial activity against *Staphylococcus aureus.* Also, some of this kind of derivatives showed anti-cancer property by binding with G-gudruplex biological structures formed in nucleic acids [16,17].

In this view, this work demonstrates the synthesis, structural and packing analysis of two indole containing azaphenantherene derivatives. The intermolecular hydrogen bonding interactions are qualified and quantified using Hirshfeld surface analysis, QTAIM (Quantum Topological Atoms In Molecules) and NCI (Non-Covalent Interaction) analyses. Also, the molecular docking analysis against main protease (M^{pro}) was carried out for the synthesized, modeled compounds and some suggested drugs for COVID-19. The docking results were then analyzed.

2. Materials and methods

2.1. Synthesis

Compounds $C_{28}H_{19}N_3$ (Ia) and $C_{29}H_{20}BrN_3O.C_2H_6OS$ (Ib) were synthesized using the procedure given below.

2.1.1. Preparation of 2-(1H-indol-3-yl)-4-phenyl-5,6-dihydrobenzo[h]quinoline-3-carbonitrile (Ia)

A mixture of 3-(1*H*-indol-3-yl)-3-oxopropanenitrile (0.1 g, 0.543 mM), 4-fluorobenzaldehyde (0.543 mM), ammonium acetate (0.1 g, 1.1 mM) and 3,4-dihydronaphthalen-1(2*H*)-one (0.543 mM) was dissolved in ethanol (10 ml) and heated to reflux on a heating mantle for 2 h. After completion of the reaction as evident from TLC, the reaction mixture was set aside at ambient temperature for 6–7 h. The precipitate formed was filtered and dried to get a pure product. The crystals were obtained from the slow evaporation technique by dissolving the product in DMSO. (Yield: 89%; m.p: 287 – 288°C). ^{1}H NMR (300 MHz, $CDCl_3$+DMSO–d_6) δ_H: 2.61–2.72 (m, 2H), 2.81 (t, *J*=7.5Hz, 2H), 7.16–7.28 (m, 3H), 7.31–7.42 (m, 4H), 7.43–7.56 (m, 4H), 8.23 (d, *J*=2.4Hz, 1H), 8.46 (d, *J*=7.2Hz, 1H), 8.49–8.57 (m, 1H), 11.42 (bs, 1H) ppm; ^{13}C NMR (75 MHz, $CDCl_3$+DMSO–d_6) δ_C: 23.4, 26.0, 101.6, 110.5, 111.9, 117.4, 119.3, 120.4, 120.9, 124.2, 124.7, 124.9, 125.7, 126.3, 126.5, 127.1,

127.2, 127.4, 128.9, 132.5, 134.6, 135.1, 137.5, 151.7, 153.1, 153.6 ppm; Anal. Calcd. for $C_{28}H_{19}N_3$: C, 84.61; H, 4.82; N, 10.57 %. Found: C, 84.66; H, 4.84; N, 10.54 %. (Fig. S1).

2.1.2. Preparation of 2-(5-bromo-1H-indol-3-yl)-4-(4-methoxyphenyl)-5,6-dihydrobenzo[h]quinoline-3-carbonitrile (Ib)

A mixture of 3-(5-bromo-1*H*-indol-3-yl)-3-oxopropanenitrile (0.1 g, 0.543 mM), 4-methoxybenzaldehyde (0.543 mM), ammonium acetate (0.1 g, 1.1 mM) and 3,4-dihydronaphthalen-1(2*H*)-one (0.543 mM) was dissolved in ethanol (10 ml) and heated to reflux on a heating mantle for 2 h. After completion of the reaction as evident from TLC, the reaction mixture was set aside at ambient temperature for 6–7 h. The precipitate formed was filtered and dried to get a pure product. The crystals were obtained from the slow evaporation technique by dissolving the product in DMSO. (Yield: 90%; m.p: 296 – 297°C). ^{1}H NMR (300 MHz, $CDCl_3$+DMSO–d_6) δ_H: 2.62–2.72 (m, 2H), 2.74–2.85 (m, 2H), 3.81 (s, 3H), 7.0 (d, *J*=8.7Hz, 2H), 7.16–7.25 (m, 3H), 7.29 (d, *J*=8.7Hz, 2H), 7.33–7.43 (m, H), 7.45–7.52 (m, 1H), 8.24 (d, *J*=3.0Hz, 1H), 8.40–8.46 (m, 1H), 8.47–8.54 (m, 1H), 11.53 (bs, 1H) ppm; ^{13}C NMR (75 MHz, $CDCl_3$+DMSO–d_6) δ_C: 23.1, 25.6, 53.3, 101.7, 110.2, 111.6, 112.3, 117.2, 119.0, 120.1, 120.6, 124.2, 124.3, 124.6, 125.4, 126.0, 126.1, 126.2, 128.4, 128.6, 132.2, 134.8, 137.2, 151.3, 152.6, 153.2, 158.0 ppm; Anal. Calcd. for $C_{29}H_{20}BrN_3O$: C, 68.78; H, 3.98; N, 8.30 %. Found: C, 68.80; H, 3.97; N, 8.33 %. (Fig. S1).

2.2. Investigation techniques

2.2.1. X-ray diffraction data

The chosen good quality crystal of compound Ia and Ib was mounted on a glass fiber using cyanoacrylate. The fiber was fixed on a goniometer head of Bruker Kappa Apex II diffractometer equipped with CCD area detector using monochromatic X-ray radiation (MoKα, λ=0.71073Å) for collecting the intensity data at room temperature available at Indian Institute of Technology (IIT), Chennai. Accurate unit cell parameters were determined from reflections of 36 frames measured in three different crystallographic zones. The intensity of each reflection is measured by $\omega/2\theta$ scan mode. The absorption correction (multi-scan) is done with SADABS [18] program. All the crystal structures were obtained using SHELXS [19] by direct methods. Full-matrix least-squares refinement procedure was used for solving structures using SHELXL [19]. All the non-hydrogen atoms were refined anisotropically and hydrogen atoms were positioned from the difference fourier maps and refined isotropically. Hydrogen atoms were positioned in calculated positions, with C-H = 0.93-0.98 Å and N-H = 0.86 Å, and allowed to ride on their respective carrier atoms, $U_{iso}(H) = 1.2U_{eq}(C)$ for CH_2, CH and NH groups. Initial structural solution showed co-crystallized completely disordered solvent molecule (DMSO) in compound Ib, which was modeled and refined using PART command along with a free variable. The solvent molecule is disordered over two sets of sites in a 0.792(2):0.208(2) ratio. The final refined structure was validated using PLATON [20] and CheckCIF routine from IuCr. Thermal ellipsoidal image and molecular packing diagrams were generated using ORTEP [21] and Mercury [22]. **CCDC 1999442 (Ia)** and **CCDC 1999443 (Ib)** contains the supplementary crystallographic data. The data can be obtained free of charge from The Cambridge Crystallographic Data Centre via www.ccdc.cam.ac.uk/structures. The crystallographic data and refinement parameters were listed in Table 1.

2.2.2. DFT and intermolecular interaction analysis

Density functional theory calculations utilizing B3LYP theory with 6-311G(d,p) [23] as a basis set was performed using ORCA 3.0.3 [24]. Frontier molecular orbital analysis was done using the optimized structure. The softwares utilized for the intermolecular interaction analysis are CrystalExplorer 3.1 [25], Multiwfn [26] and NCIPLOT [27]. The results are visualized using VMD [28]. The procedure and principles behind the Hirshfeld surface analysis, QTAIM and NCI can be found somewhere else [29].

2.2.3. Preparation of ligands and its docking

A ligand database was created containing more than 300 molecules of suggested COVID-19 drugs (www.drugbank.ca/), and some modeled derivatives of azaphenantherene. All the ligand molecules were energy minimized using Steepest descent algorithm employed in Avogadro [30]. The PDB (Protein Data Bank) file of the macromolecule (6LU7) was retrieved from RCSB protein data bank (https://www.rcsb.org/). The active pocket of the protein was predicted using CASTp server (http://sts.bioe.uic.edu/castp/). The water molecules were removed, if any, from the protein molecule. A grid box with the size $23.656 \times 25.926 \times 27.932$ with coordinates (x,y,z) of -11.493, 15.366, 69.444 having the grid spacing of 0.375Å was used. The docking Lamarckian Genetic Algorithm (LGA) was allowed to produce 10 docked positions for each ligand. Molecular docking studies were performed using AutoDock vina [31] in PyRx [32] software. The final results were analyzed and visualized on the basis of docking scores using Chimera [33] software.

3. Data, value and validation

3.1. Molecular structural features in the single crystals (Ia) and (Ib)

The two compounds differ by the substituent either in fourth position or in the sixth position of the azaphenantherene ring. This substitution does not affect the crystal system. The ORTEP diagrams with thermal ellipsoids at 30% probability with an atom numbering scheme for Ia and Ib are shown in Fig. 2 and 3.

Table 1
Crystallographic table of Compounds Ia and Ib

	Compound - Ia	Compound - Ib
Empirical formula	C_{28} H_{19} N_3	C_{29} H_{20} Br N_3 O, C_2 H_6O S
Molecular weight	397.46	584.52
Temperature (K)	293(2)	293(2)
Wavelength (Å)	0.71073	0.71073
Crystal system	Triclinic	Triclinic
Space group	P -1	P -1
a (Å)	9.3339(7)	10.5600(3)
b (Å)	10.4957(8)	11.2058(3)
c (Å)	12.2704(8)	12.7280(3)
α (°)	82.964(3)°	83.158(2)°
β (°)	71.834(3)°	78.515(2)°
γ (°)	64.713(3)°	69.156(2)°
Volume (Å^3)	1032.64(13)	1377.47(7)
Z	2	2
Density (calculated) (mg/m^3)	1.278	1.409
Absorption coefficient (mm^{-1})	0.076	1.601
F(000)	416	600
Crystal size (mm^3)	0.2 × 0.15 × 0.1	0.2 × 0.15 × 0.1
Theta range for data collection (°)	2.521 to 26.563	2.322 to 26.728
Index ranges	-11<=h<=11,-13<=k<=13,-15<=l<=15	-13<=h<=13,-14<=k<=14,-16<=l<=16
Reflections collected	20120	32037
Independent reflections	4201[R(int) = 0.0390]	5834[R(int) = 0.0372]
Completeness to theta = 25.242°	98.6%	99.9%
Refinement method	Full-matrix least-squares on F2	Full-matrix least-squares on F2
Data / restraints / parameters	4201 / 0 / 280	5834 / 0 / 375
Goodness-of-fit on F2	1.021	1.002
Final R indices [I>2sigma(I)]	R1 = 0.0538,wR2 = 0.1235	R1 = 0.0383,wR2 = 0.0778
R indices (all data)	R1 = 0.1012,wR2 = 0.1465	R1 = 0.0826,wR2 = 0.0936
Extinction coefficient	n/a	n/a
Largest diff. peak and hole (e.Å^{-3})	0.271 and -0.200	0.272 and -0.396

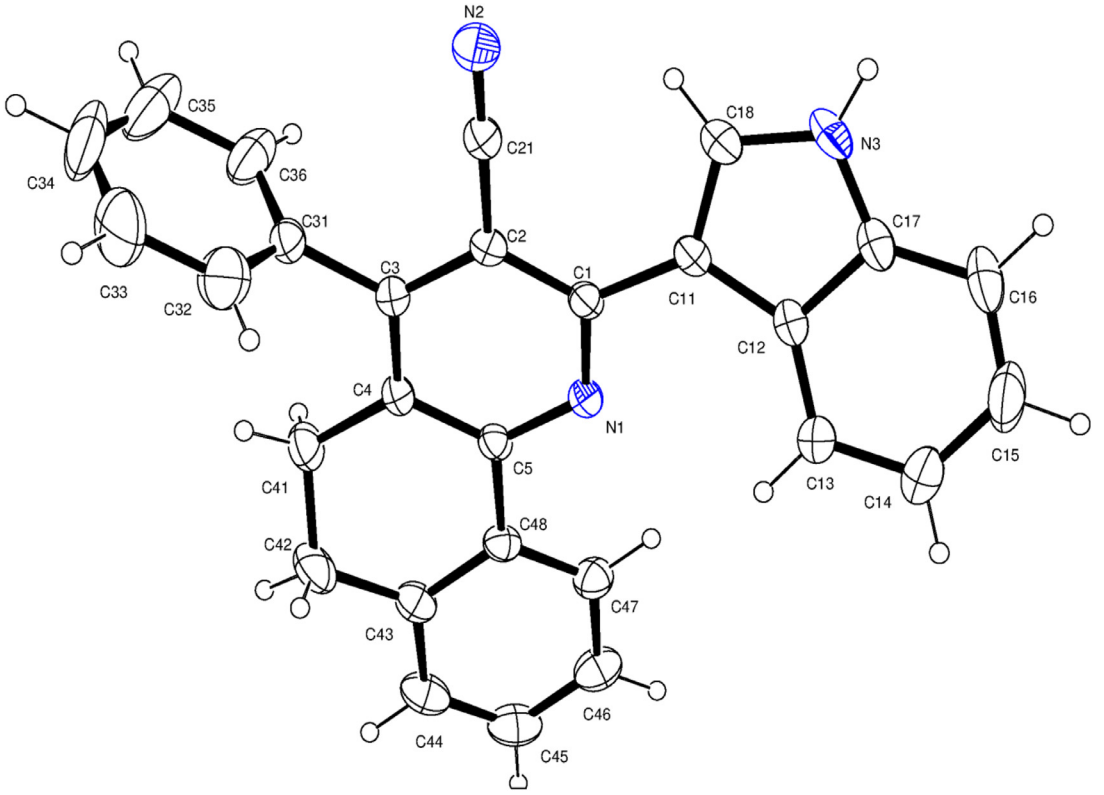

Fig. 2. ORTEP diagram of Ia showing 30% probability and atom-numbering scheme

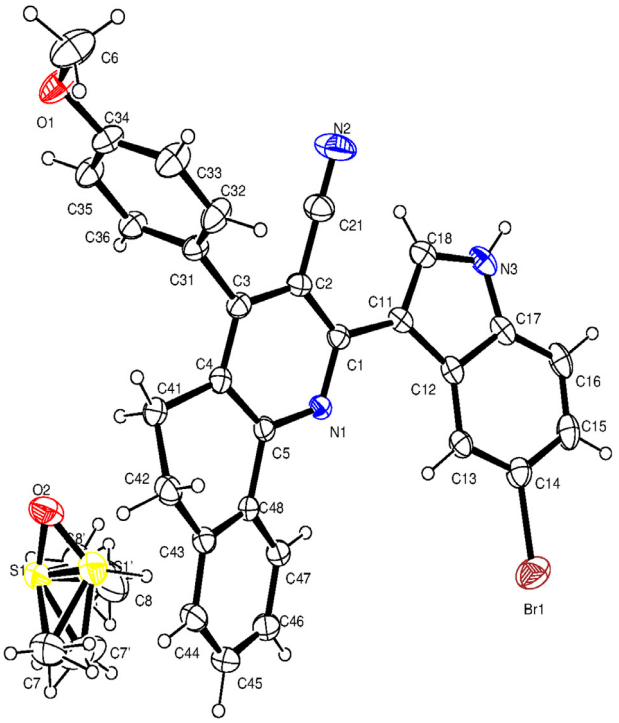

Fig. 3. ORTEP diagram of Ib showing 30% probability and atom-numbering scheme

The bond lengths and angles of azaphenantherene ring are very much similar to the reported structures [34–40]. The 14-membered ring (C1-C5/C41-C48/N1) is significantly deviated from planarity (r.m.s deviation of 0.1519(1) Å in (Ia) and 0.2278(2) Å in (Ib) with the fitted atoms). The atoms C41 [(0.3391(2) Å in (Ia) & -0.4577(2) Å in (Ib)] and C42 [(-0.2993(1) Å in (Ia) & 0.3585(2) Å in (Ib)] have the maximum out of plane deviation. The phenyl ring (C43-C48) ethylenic bridged with cyclohexadiene is nearly a planar, forming an interplanar angle of 11.41(3)° in (Ia) and 20.86(2)° in (Ib). This twist may be due to the saturation at C41 – C42 and the absence of steric pressure at N1 force the bay angles at C41 and C42 to adopt sp^2 values. Further, the cyclohexadiene ring adopts screw boat conformation [$Q_2 = 0.335(1)$ Å, $\theta = 63.8(5)°$ and $Q_T = 0.374(1)$ Å] [34] in compound (Ia) and distorted screw boat [$Q_2 = 0.434(2)$ Å, $\theta = 68.1(2)°$ and $Q_T = 0.467(2)$ Å] in compound (Ib) evidenced from the puckering parameters [41]. The pyridine ring (N1/C1-C5) is a planar with the maximum deviation of 0.0082(2) Å in (Ia) and 0.0061(3) Å in (Ib) with the fitted atoms.

The C2 – C21 bond length in compounds Ia and Ib are 1.437(3) Å and 1.442(3) Å, which signifies the aromatic type bond length, the bond distance N2 – C21 is 1.139(2) Å in (Ia) and 1.139(3) Å in (Ib) indicates the triple bond nature [34]. The angle around C21 [178.7(2)° in (Ia) and 179.6(3)° in (Ib)] defines the linearity of the nitrile group. The deviation of C21 and N2 atoms from the mean plane of pyridine [0.033(3) Å & 0.038(3) Å in (Ia) and 0.053(2) Å & 0.099(4) Å in (Ib)] defines the coplanarity. These deviations are due to the nearby substitutions in the pyridine ring.

The indole ring (N3/C11-C18) in both the compounds is planar with the r.m.s deviation of 0.0164(2) Å in (Ia) and 0.0146(2) Å in (Ib) with the fitted atoms. The sum of the angles around N3 is 360(2)° in both the compounds, which indicates the sp^2 hydridization.

The indole ring in both the compounds is in (-) *syn-periplanar* conformation with the pyridine ring evidenced from the torsion N1-C1-C11-C12 [-20.2(2)° in (Ia) and -20.1(3)° in (Ib)]. The indole in all the compounds are nearly coplanar with the pyridine which may be seen from the dihedral angle [22.75(3)° and 20.71(4)° in compounds Ia and Ib respectively].

The bond lengths and angles of anisole ring are consistent with the similar structure [42] but the phenyl ring deviates from the normally observable values [34–37,43]. From the torsion C2-C3-C31-C32 the phenyl substituent at C3 in the compound Ia [-95.4(3)°] is in (-) anti-clinal and anisole in compound Ib [107.8(3)°] is in (+) anti-clinal conformation. The substitutions are nearly perpendicular to the pyridine ring [84.14(3)° in (Ia) and 73.64(3)° in (Ib)].

The molecular structure of compound Ia is stabilized through an intermolecular interaction N3-H3…N2. (Table 2 and Fig. 4). The interaction from indole (N3-H3) to cyano nitrogen ($N2^i$ [symmetry code: (i) 2-x, 1-y, 1-z]) connects the inversely related molecules thus forming an [$R_2^2(16)$] [44] lying along the (110) plane. This motif is a characteristic motif of indole and nitrile containing compounds [45–48].

In compound Ib, the host and guest molecules are forming an intermolecular interaction thus stabilizing the crystal. Here the characteristic ring motif was not found because of the strong interaction with the solvent (DMSO) molecule. The atoms

Table 2
Hydrogen bonds for Ia [Å and °]

D-H...A	d(D-H)	d(H...A)	d(D...A)	<(DHA)
N(3)-H(3)...N(2)#1	0.86	2.19	3.038(3)	170

Symmetry transformations used to generate equivalent atoms:
#1 2-x, 1-y, 1-z

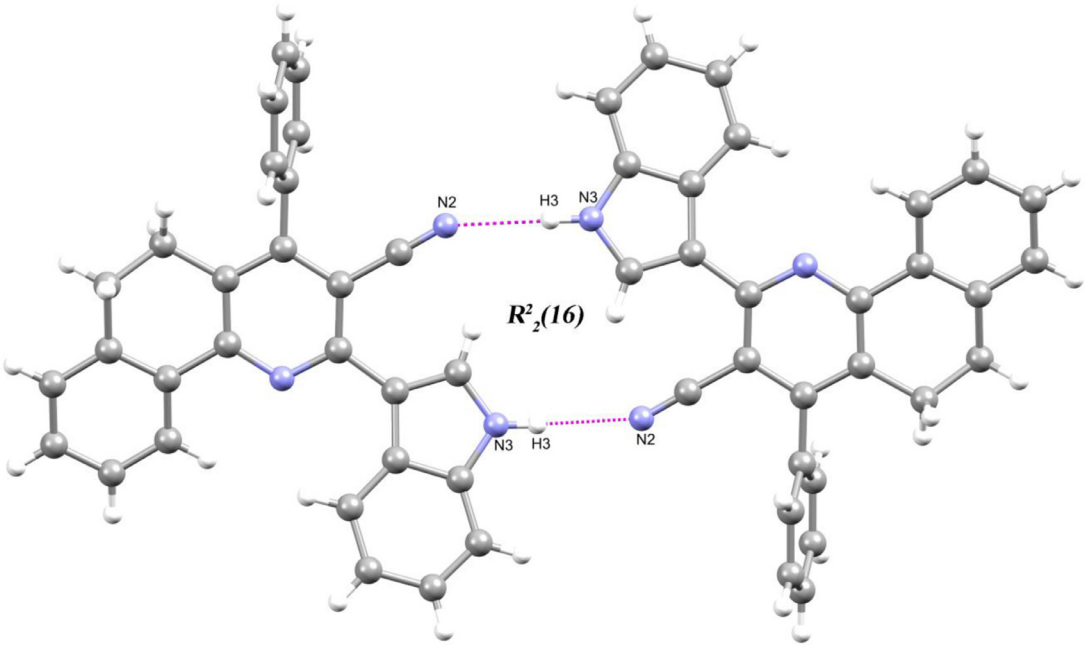

Fig. 4. Partial packing diagram of Ia showing $\boldsymbol{R}_2^2(16)$ring motifs

Table 3
Hydrogen bonds for Ib [Å and °]

D-H...A	d(D-H)	d(H...A)	d(D...A)	<(DHA)
N(3)-H(3)...O(2)#1	0.86	1.91	2.754(3)	168
C(34)-H(34)...O(2)#2	0.93	2.63	3.545(4)	170

Symmetry transformations used to generate equivalent atoms:
#1 –x, 1-y, 1-z #2 -x,-y+1,-z+2

Table 4
Contribution of individual interactions to Hirshfeld surface

Compound	H – H(%)	C-H/H-C (%)	N-H/H-N (%)	Br-H/H-Br (%)	O-H /H-O (%)	C-C (%)	C-N /N-C (%)
Ia	51.9	26.9	11.5	-	-	6.6	3.2
Ib	42.6	22.5	10.1	9.8	8.6	-	-

N3 and C34 act as donors and O2 in DMSO act as an acceptor (Table 3). The two interactions N3-H3...O2^{i} [symmetry code: (i) –x, 1-y, 1-z] and C34-H34...O2^{ii} [symmetry code: (ii) -x,-y+1,-z+2] forming a chain motif of $C_2^1(12)$ (Fig. 5).

3.2. Hirshfeld surface, QTAIM and NCI analysis

Hirshfeld surface of compounds Ia and Ib are mapped over d_{norm} surface shown in Fig. S2 and S3 respectively. Table 4 shows the individual contributions. The colour coded NCI plot along with QTAIM critical points of compounds Ia and Ib are shown in Fig. S4 and S5 and the values of QTAIM descriptors are shown in Table 5 and 6.

In both the structures, apparently short contacts seem to influence H-H interaction (Table 4). Other significant contributions are from C-H, N-H and O-H interactions. These arise due to the intermolecular interactions present in the compounds. Further contributions are may be due to *van der Waals* interactions.

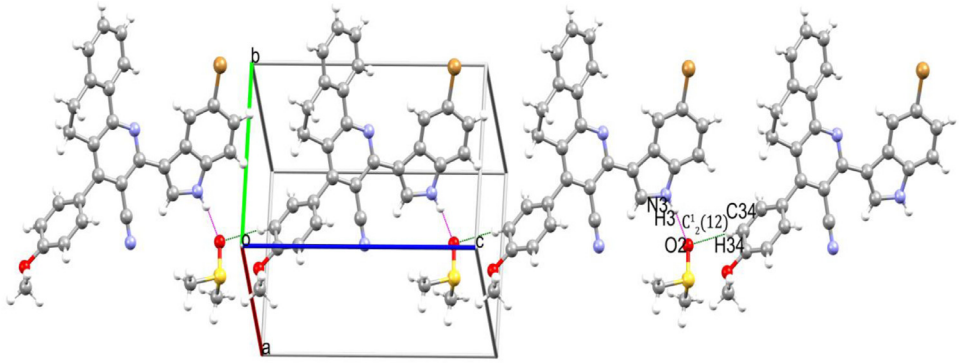

Fig. 5. Partial packing diagram of Ib showing $C_2^1(12)$chain motifs

Table 5
QTAIM descriptors for Ia

Interaction	ρa.u	$\nabla^2\rho$a.u	G(r)a.u	V(r)a.u	H(r)a.u	$\frac{\lvert V(r)\rvert}{G(r)}$	E_{bond} kJ.mol^{-1}
N3-H3...N2 #1	0.0167	0.0531	0.0118	-0.0104	0.0015	0.881	-15.396

Symmetry transformations used to generate equivalent atoms:
#1 2-x, 1-y, 1-z

Table 6
QTAIM descriptors for Ib

Interaction	ρa.u	$\nabla^2\rho$a.u	G(r)a.u	V(r)a.u	H(r)a.u	$\frac{\lvert V(r)\rvert}{G(r)}$	E_{bond} kJ.mol^{-1}
N3-H3...O2 #1	0.0296	0.1037	0.024	-0.0227	0.0016	0.946	-30.791
C34-H34...O2 #2	0.0078	0.0222	0.0054	-0.0052	0.0003	0.963	-7.054

Symmetry transformations used to generate equivalent atoms:
#1 –x, 1-y, 1-z #2 -x,-y+1,-z+2

Hirshfeld surface shows two and four red spots for compounds Ia and Ib respectively (Fig. S2 and S3). In compound Ia, for N–H...N interaction, $d_i + d_e \approx 2.0$ Å which is less than the sum of the *van der Waals* radii 2.74 Å [49,50] indicated as bright red spots (Fig. S2). These interactions are colour coded as blue in NCI index indicating strong interactions (Fig. S4). The energy of this interaction from QTAIM descriptors is found to be -15.396 kJ/mol (Table 5). The 'sign(λ_2)ρ' values are -0.0167 a.u.

In compound Ib, for N–H...O interaction, $d_i + d_e \approx 1.7$ Å which is less than the sum of the *van der Waals* radii 2.61 Å. The energy of this interaction is -30.791 kJ/mol (Table 6) with the 'sign(λ_2)ρ' value of -0.0278 a.u. and there is an additional C – H ... O interaction, which is indicated as a light red spot in Hirshfeld surface and in NCI index it is colour coded as green (Fig. S3 and S5). For the C – H ... O interactions, $d_i + d_e \approx 1.8$ Å which is less than the sum of the *van der Waals* radii 2.61 Å [49,50]. The energy of this interaction is found as -7.054 kJ/mol, with 'sign(λ_2)ρ' value of -0.0078 a.u. The green coloured isosurfaces corresponds to H...H *van der Walls* interaction.

From this analysis, it can be concluded that the compound Ib forms a stronger interaction (N3-H3...O2) with the solvent molecule.

3.3. HOMO-LUMO analysis

The studies on frontier molecular orbital reveal the chemical reactivity, chemical hardness or softness of the molecule and kinetic stability [51].

It can be seen from Fig. 6 that the HOMO orbitals are located on both the cyanopyridine and indole moieties while LUMO orbitals are located on azaphenantherene, nitrile group and substituted aryl rings. Therefore the substitution has an influence on the electron accepting ability of the compounds. All the calculated energy parameters along with a log P and dipole moment are given in Table 7.

The ionization potential (I) and electron affinity (A) for compound Ia is much lesser than for compound Ib. This makes compound Ia more reactive than compound Ib. This is further confirmed by low chemical hardness (η) and high softness (S) of compound Ia as compared with Ib. Based on the values of electronegativity (χ) and chemical potential (μ), the compound Ia has more electron attracting ability than Ib and this is supplemented by the high electrophilicity index (ω) of Ib. Cell membrane permeability of compound Ib is higher than Ia, this indicates the higher lipophilicity index of compound Ib. The

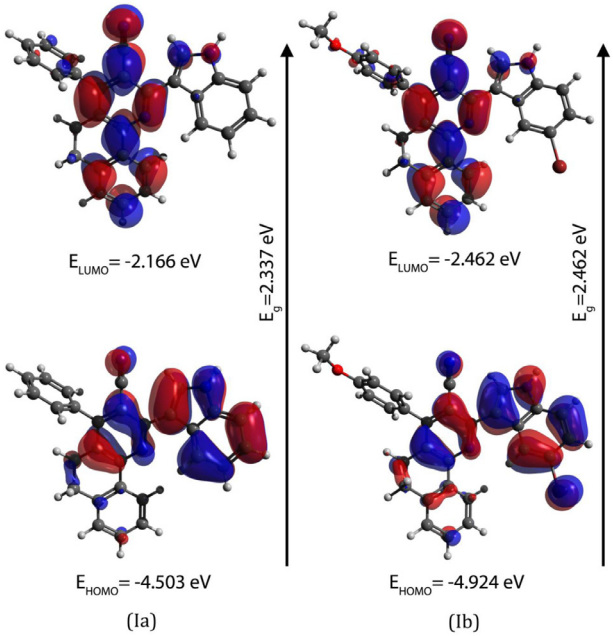

Fig. 6. Frontier molecular orbitals and energies of the HOMO, LUMO

Table 7
Calculated energy values by B3LYP/6-311G(d,p) level

Parameters	Compound - Ia	Compound - Ib
E_{HOMO} (eV)	-4.503	-4.924
E_{LUMO} (eV)	-2.166	-2.462
Ionization potential (I) ($I = -E_{HOMO}$) (eV)	4.503	4.924
Electron affinity (A) ($A = -E_{LUMO}$) (eV)	2.166	2.462
Energy gap (ΔE) (eV)	2.337	2.462
Electronegativity (χ) ($\chi = \frac{(I+A)}{2}$) (eV)	3.335	3.693
Chemical potential (μ) ($\mu = -\frac{(I+A)}{2}$) (eV)	-3.335	-3.693
Chemical hardness (η) ($\eta = \frac{(I-A)}{2}$) (eV)	1.083	1.231
Chemical softness (S) ($S = \frac{1}{2\eta}$) (eV)	0.462	0.406
Electrophilicity index (ω) ($\omega = \frac{\mu^2}{2\eta}$) (eV)	5.135	5.54
log P	3.88	4.05
Dipole moment (debye)	1.747	2.968

value of the dipole moment, which signifies the ligand-protein interaction on the basis of electrostatic interaction, is much higher in compound Ib than Ia.

Both the compounds are reducers based on the negative HOMO and LUMO values and may undergo oxidative reactions with cytochrome P450 enzyme [52].

3.4. Molecular docking analysis

One of the SARS (Severe Acute Respiratory Syndrome) CoV-2 (Coronavirus-2) enzyme, main protease (M^{pro}) or 3-chymotrypsin like protease ($3CL^{pro}$) along with a peptide like N3 inhibitor was first made available on 5th Febrauary 2020 [53]. This enzyme helps in the viral replication through RNA translation [54]. This is an ideal target for drug designing in the combat of COVID-19 (Coronavirus disease-2019) since; there is no similar enzyme in human [53]. Generally protease inhibiting drugs targeting the hydrophobic pockets [55]. The catalytic residues of this enzyme are formed by a dyad His41-Cys145 which is in the hydrophobic region of the active pocket [56].

All the ligand molecules were docked in the active site and results are given as Fig. 7, Table 8, S1 and S2. The peptide like inhibitor N3formed interactions with the amino acids, His 41, Phe 140, Asn 142, His 163, His 164, Glu 166, Gln 189 and Thr 190 [57]. Both the synthesized compounds (Ia and Ib) show the similar kind of behavior in the active pocket of possessing same hydrogen bonding interactions (Fig. 7). The difference in the conformations of pyridine in Ia and Ib plays a role. This difference clearly alters the hydrogen bond distance, which is reflected in the binding energy. Clearly, the screw boat conformation (Ia) forms relatively stronger interaction with high binding energy (-9.4 kcal/mol) than the distorted (Ib)

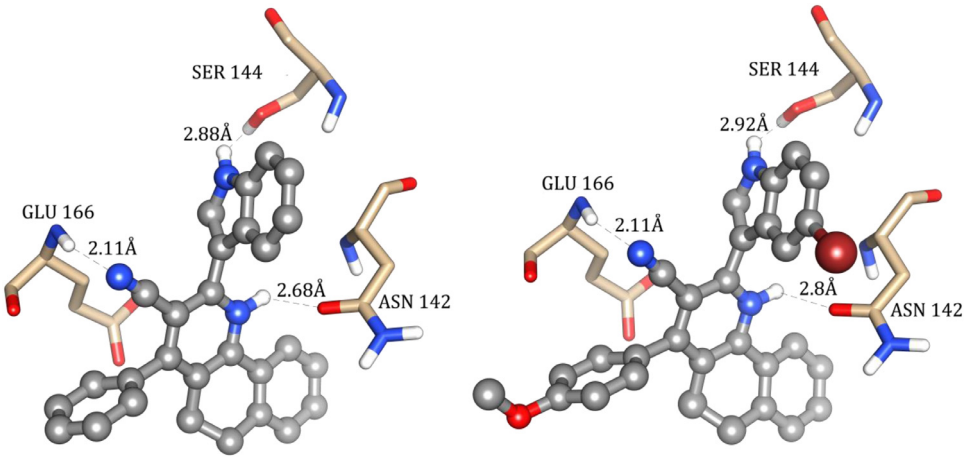

Fig. 7. The interactions between the synthesized compounds Ia (left) and Ib (right) with the amino acids of SARS CoV-2 main protease

Table 8
Azaphenantherene derivatives with binding energy and Lipinski's rule of 5 criteria

Compound	M. wt(g/mol)	No. of H-bond donors	No. ofH-bond acceptors	log P	Hydrogen bond (docking)	Distance (Å)	B.E (kcal/mol)	Lipinski's rule violations
8	397.47	1	2	3.88	ASN 142SER 144GLU 166	2.682.882.11	**-9.4**	0
9	506.39	1	3	4.05	ASN 142SER 144GLU 166	2.82.922.11	-8.7	1

conformation (-8.7 kcal/mol) (Table 8). Both the compounds filled the active pocket and resides exactly above the catalytic residues, thus blocks the substrate binding (Fig. S6).

Among the virtually screened drugs, Lopinavir showed the maximum binding energy (-10.1 kcal/mol) with two interactions (Gly 143, Glu 166). Ribavirin bounds tightly inside the active pocket through seven interactions with six amino acids (Table S1). Among the six residues four residues are same as that of N3. Favipiravir (-5.0), Galidesivir (-7.2), Hydroxychloroquine (-6.4), Remesesvir (-8.5), Umifenovir (-7.1) formed minimum two interactions.

The modeled compounds were interacted in the similar fashion as that of the synthesized compounds. The compound M-2 having the highest binding energy (-9.0 kcal/mol; 2 interactions) and M-4 having the highest interactions (-8.2 kcal/mol; 6 interactions) (Table. S2).

4. Conclusion

In this work, two azaphenantherene derivatives differ by the substituent either in fourth position or in the sixth position were synthesized. Their structures were elucidated using SXRD. The substitution does not affect the crystal system, but changes the physicochemical properties. From the intermolecular interaction analyses, the compound Ib was found to have very strong interaction of -30.791 kJ/mol with the solvent DMSO molecule. Based on the electronegativity, electrophilicity index and dipole moment, it is concluded that compound Ib showed better drug-like properties than Ia. Docking analysis suggests that, the drugs Lopinavir and Ribavirin can be used as an inhibitor of SARS CoV-2 main protease. Also, the synthesized compounds Ia, Ib and modeled compounds M-2 and M-4 were found to be occupied the active pocket and interact with the amino acids confirmed their efficacy of inhibiting M^{pro}. However, further *in-vitro* and *in-vivo* analyses around these mentioned compounds are required to ascertain these suggestions.

Declaration of Competing Interests

The authors declare no conflict of interest

Acknowledgements

JS thanks the UGC for funds under project No. MRP-7018/16 (SERO/UGC). JS and MV thank the management of The Madura College for their encouragement and support.

Supplementary materials

Supplementary material associated with this article can be found, in the online version, at doi:10.1016/j.cdc.2020.100470.

References

[1] N.J. White, Clinical pharmacokinetics of antimalarial drugs, Clin. Pharmacokinet. 10 (1985) 187–215.
[2] K.J. Palmer, S.M. Holliday, R.N. Brogden, Mefloquine. A review of its antimalarial activity, pharmacokinetic properties and therapeutic efficacy, Drugs 45 (1993) 430–475.
[3] K. Raynes, M. Foley, L. Tilley, L.W. Deady, Novel bisquinoline antimalarials: synthesis, antimalarial activity, and inhibition of haem polymerization, Biochem. Pharmacol. 52 (1996) 551–559.
[4] K. Chibale, J.R. Moss, M. Blackie, D. Schalkwyk, P.J. Smith, New amine and urea analogs of ferrochloroquine: synthesis, antimalarial activity in vitro electrochemical studies, Tetrahedron Lett. 41 (2000) 6231–6235.
[5] A.H. Abadi, G.H. Hegazy, A.A.E. Zaher, Synthesis of novel 4-substituted-7-trifluoromethylquinoline derivatives with nitric oxide releasing properties and their evaluation as analgesic and anti-inflammatory agents, Bioorg. Med. Chem. 13 (2005) 5759–5765.
[6] L.A. Martin, J.E. Head, S. Pancholi, J. Salter, E. Quinn, S. Detre, S. Kaye, A. Howes, M. Dowsett, S.R. Johnston, The farnesyltransferase inhibitor R115777 (tipifarnib) in combination with tamoxifen acts synergistically to inhibit MCF-7 breast cancer cell proliferation and cell cycle progression in vitro and in vivo, Mol. Cancer Ther. 6 (2007) 2458–2467.
[7] N. Yoshimura, S. Kudoh, T. Kimura, S. Mitsuoka, K. Matsuura, K. Hirata, K. Matsui, S. Negoro, K. Nakagawa, M. Fukuoka, EKB-569, a new irreversible epidermal growth factor receptor tyrosine kinase inhibitor, with clinical activity in patients with non-small cell lung cancer with acquired resistance to gefitinib, Lung Cancer 51 (2006) 363–368.
[8] A. Mai, D. Rotili, D. Tarantino, A. Nebbioso, S. Castellano, G. Sbardella, M. Tini, L. Altucci, Identification of 4-hydroxyquinolines inhibitors of p300/CBP histone acetyltransferases, Bioorg. Med. Chem. Lett. 19 (2009) 1132–1135.
[9] D.A. Scott, C.L. Balliet, D.J. Cook, A.M. Davies, T.W. Gero, C.A. Omer, S. Poondru, M.E. Theoclitou, B. Tyurin, M.J. Zinda, Identification of 3-amido-4-anilinoquinolines as potent and selective inhibitors of CSF-1R kinase, Bioorg. Med. Chem. Lett. 19 (2009) 697–700.
[10] R.S. Upadhayaya, J.K. Vandavasi, N.R. Vasireddy, V. Sharma, S.S. Dixit, J. Chattopadhyaya, Design, synthesis, biological evaluation and molecular modelling studies of novel quinoline derivatives against mycobacterium tuberculosis, Bioorg. Med. Chem. 17 (2009) 2830–2841.
[11] A.R. Gholap, K. S., F.Shirazi Toti, R. Kumari, M.K. Bhat, M.V. Deshpande, K.V. Srinivasan, Synthesis and evaluation of antifungal properties of a series of the novel 2-amino-5-oxo-4-phenyl-5,6,7,8-tetrahydroquinoline-3-carbonitrile and its analogues, Bioorg. Med. Chem. 15 (2007) 6705–6715.
[12] S. Massari, D. Daelemans, G. Manfroni, S. Sabatini, O. Tabarrini, C. Pannecouque, V. Cecchetti, Studies on anti-HIV quinolones: New insights on the C-6 position, Bioorg. Med. Chem. 17 (2009) 667–674.
[13] C. Willemann, R. Grunert, P.J. Bednarski, R. Troschutz, Synthesis and cytotoxic activity of 5,6-heteroaromatically annulated pyridine-2,4-diamines, Bioorg. Med. Chem. 17 (2009) 4406.
[14] A. Zarghi, R. Ghodsi, E. Azizi, B. Daraie, M. Hedayati, O.G. Dadrass, Synthesis and biological evaluation of new 4-carboxyl quinoline derivatives as cyclooxygenase-2 inhibitors, Bioorg. Med. Chem. 17 (2009) 5312.
[15] A. Cappelli, G. Giuliani, A. Gallelli, S. Valenti, M. Anzini, L. Mennuni, F. Makovec, A. Cupello, S. Vomero, Structure-affinity relationship studies on arylpiperazine derivatives related to quipazine as serotonin transporter ligands. Molecular basis of the selectivity SERT/5HT3 receptor, Bioorg. Med. Chem. 13 (2005) 3455.
[16] H. Paritala, S.M. Firestine, Benzo(h)quinoline derivatives as G-quadruplex binding agents, Bioorg. Med. Chem. Lett. 19 (2009) 1584.
[17] L.H. Hurley, R.T. Wheelhouse, D. Sun, S.M. Kerwin, M. Salazar, O.Y. Fedoroff, F.X. Han, H. Han, E. Izbicka, D.D. Von Hoff, G-quadruplexes as targets for drug design, Pharmacol. Ther. 85 (2000) 141.
[18] Bruker, SADABS, BRUKER AXS Inc., Maddison, Wisconsin, USA, 1998.
[19] G.M. Sheldrick, Crystal structure refinement with SHELXL, Acta Cryst. C 71 (2015) 3–8.
[20] A.L. Spek, Structure validation in chemical crystallography, Acta Cryst. D. 65 (2009) 148–155.
[21] L.J. Farrugia, ORTEP-3 for windows - a version of ORTEP-III with a graphical user interface (GUI), J. Appl. Cryst. 30 (1997) 565.
[22] C.F. Macrae, I.J. Bruno, J.A. Chisholm, P.R. Edgington, P. McCabe, E. Pidcock, L. Rodriguez-Monge, R. Taylor, J. van de Streek, P.A. Wood, Mercury CSD 2.0 - new features for the visualization and investigation of crystal structures, J. Appl. Cryst. 41 (2008) 466–470.
[23] M.J. Frisch, J.A. Pople, J.S. Binkley, Self-consistent molecular orbital methods 25. Supplementary functions for Gaussian basis sets, J. Chem. Phys. 80 (1984) 3265.
[24] F. Neese, The ORCA program system *Wiley Interdiscip*, Rev.: Comput. Mol. Sci. 2 (2012) 73–78.
[25] S. K. Wolff, D. J. Grimwood, J. J. McKinnon, M. J. Turner, D. Jayatilaka and M. A. Spackman, CrystalExplorer (Version 3.1), University of Western Australia, 2012.
[26] T. Lu, F. Chen, MULTIWFN: a multifunctional wavefunction analyzer, J. Comp. Chem. 33 (2012) 580–592.
[27] J. Contreras-García, E.R. Johnson, S. Keinan, R. Chaudret, J.-P. Piquemal, D.N. Beratan, W. Yang, NCIPLOT: a program for plotting non covalent interaction regions, J. Chem. Theor. Comp. 7 (2011) 625–632.
[28] W. Humpherey, A. Dalke, K. Schulten, VMD: visual molecular dynamics, J. Mol. Graph. 14 (1996) 33–38.
[29] M. Venkateshan, J. Suresh, Synthesis, physicochemical and quantum chemical studies on a new organic NLO crystal: cinnamoylproline, J. Mol. Struct. 1180 (2019) 826–838.
[30] M.D. Hanwell, D.E. Curtis, D.C. Lonie, T. Vandermeersch, E. Zurek, G.R. Hutchison, Avogadro: an advanced semantic chemical editor, visualization, and analysis platform, J. Cheminform. 4 (2012) 17.
[31] O. Trott, A.J. Olson, AutoDock Vina: Improving the speed and accuracy of docking with a new scoring function, efficient optimization, and multithreading, J. Comp. Chem. 31 (2010) 455–461.
[32] S. Dallakyan, A.J. Olson, Small-molecule library screening by docking with PyRx, Methods Mol. Bio. 1263 (2015) 243–250.
[33] E.F. Pettersen, T.D. Goddard, C.C. Huang, G.S. Couch, D.M. Greenblatt, E.C. Meng, T.E. Ferrin, UCSF chimera - a visualization system for exploratory research and analysis, J. Comput. Chem. 25 (2004) 1605–1612.
[34] A.S. Girgis, M.N. Aziz, E.M. Shalaby, F.M. Asaada, I.S. Ahmed Farag, Synthesis and X-ray studies of novel azaphenanthrenes, J. Chem. Res. 42 (2018) 90–95.
[35] A.M. Asiri, A.O. Al-Youbi, H.M. Faidallaha, S. Weng, Ng. 2-Amino-4-(4-chlorophenyl)-5,6-dihydrobenzo[h]quinoline-3-carbonitrile–3-amino-1-(4-chlorophenyl)-9,10-dihydrophenanthrene-2,4-dicarbonitrile (1/4), Acta Cryst. E 67 (2011) o2872.
[36] X. Wang, D. Shi, S. Tua, K. Yu, 2-Amino-4-phenyl-5,6-dihydrobenzo[h]quinazoline, Acta Cryst. E 59 (2003) o423–o424.
[37] M.E. Haiba, E.S. Al-Abdullah, H.A. Ghabbour, S.M. Riyadh, R.M. Abdel-Kader, Inhibitory activity of benzo[h]quinoline and benzo[h]chromene in human glioblastoma cells, Trop. J. Pharm. Res. 15 (2016) 2337–2343.
[38] G.E.H. Elgemeie, N.M. Fathy, P.G. Jone, 2-Amino-4-(4-chlorophenyl)-5,6-dihydrobenzo[h]quinoline-3-carbonitrile, a strongly fluorescent phenanthridine analogue, Acta Cryst. C 54 (1998) 1314–1316.
[39] J.Q. Wang, S.G. Tang, C. Guo, 2-Amino-4-(4-fluorophenyl)-6-(naphthalen-1-yl)pyridine-3-carbonitrile, Acta Cryst. E 67 (2011) o56.
[40] A.M. Asiri, H.M. Faidallah, K.A. Alamry, S. Weng Ng., E.R.T. Tiekink, 3-Amino-1-(3,4-dimethoxyphenyl)-9,10-dihydrophenanthrene-2,4-dicarbonitrile, Acta Cryst. E 68 (2012) o1118–o1119.
[41] D. Cremer, J.A. Pople, General definition of ring puckering coordinates, JACS 97 (1975) 1354–1358.
[42] J. Portilla, C. Lizarazo, J. Cobo, C. Glidewel, A [pi]-stacked chain of hydrogen-bonded dimers in 3-tert-butyl-1-(4-chlorophenyl)-4-phenylindeno[1,2-b] pyrazolo[4,3-e]pyridin-5(1H)-one and a [pi]-stacked sheet of hydrogen-bonded chains in 3-tert-butyl-1-(4-chlorophenyl)-4-(4-methoxyphenyl)indeno [1,2-b]pyrazolo[4,3-e]pyridin-5(1H)-one, Acta Cryst. C 67 (2011) o479–o483.
[43] H.F. Gonzalez, M. Blanco-Lomas, L. Rivado-Casas, M.A. Rodriguez, P.J. Campos, D. Sampedro, Addition of oxime derivatives to alkynyl fischer carbine complexes, Organometallics 31 (2012) 6572–6581.

[44] J. Bernstein, R.E. Davis, L. Shimoni, N. Chang, Patterns in hydrogen bonding: functionality and graph set analysis in crystals, Angew. Chem. Int. Ed. Engl. 34 (1995) 1555–1573.
[45] a P. Ramesh, A. Subbiahpandi, P. Thirumurugan, P.T. Perumal, M.N. Ponnuswamy, 4-(4-Bromophenyl)-6-(1H-indol-3-yl)-2,2′-bipyridine-5-carbonitrile, Acta Cryst. E 65 (2009) o450. b. P. Ramesh, A. Subbiahpandi, P. Thirumurugan, P. T. Perumal, and M. N. Ponnuswamy, 4-(2,4-Dichlorophenyl)-2-(1H-indol-3-yl)-6-(2-pyridyl)-1,4-dihydropyridine-4-carbonitrile, *Acta Cryst. E.* 64 (2008) o1891. c. P. Ramesh, A. Subbiahpandi, P. Thirumurugan, P., T. Perumal, and M. N. Ponnuswamy, 4-(2,4-Dichlorophenyl)-6-(1H-indol-3-yl)-2,2′;-bipyridine-5-carbonitrile, *Acta Cryst. E.* 65(2009) o996 – o997.
[46] W. Zhu, Y. Xiang, S. Zhu, 6-(1H-Indol-3-yl)-4-phenyl-2,2′-bipyridine-5-carbonitrile, Acta Cryst. E 65 (2009) o1187.
[47] G. Vimala, N. Poomathi, Y. AaminaNaaz, P.T. Perumal, A. SubbiahPandi, Crystal structure of 5-(5-chloro-2-hydroxybenzoyl)-2-(2-methyl-1H-indol-3-yl) nicotinonitrile, Acta Cryst. E 71 (2015) o822–o823.
[48] a R. Vishnupriya, J. Suresh, S. Bharkavi, S. Perumal, P.L. Nilantha Lakshman, Crystal structure of 2-(2-bromophenyl)-4-(1H-indol-3-yl)-6-(thiophen-2-yl) pyridine-3-carbonitrile, Acta Cryst. E 70 (2014) o968–o969. b. R. Vishnupriya, J. Suresh, P. Gunasekaran, S. Perumal, and P. L. N. Nilantha Lakshman, Crystal structure of 2-(4-chlorophenyl)-4-(1H-indol-3-yl)-6-phenylpyridine-3-carbonitrile, *Acta Cryst. E.* 70 (2014) o978.
[49] A. Bondi, van der Waals volumes and radii, J. Phys. Chem. 68 (1964) 441–451.
[50] R.S. Rowland, R. Taylor, Intermolecular nonbonded contact distances in organic crystal structures: comparison with distances expected from van der Waals radii, J. Phys. Chem. 100 (1996) 7384–7391.
[51] B. Babu, J. Chandrasekaran, B. Mohanbabu, Y. Matsushita, M. Saravanakumar, Growth, physicochemical and quantum chemical investigations on 2-amino 5-chloropyridinium 4-carboxybutanoate – an organic crystal for biological and optoelectronic device applications, RSC Adv. 6 (2016) 110884–110897.
[52] M. Salihovic, S. Huseinovic, S. Spirtovic-Halilovic, A. Osmanovic, A. Dedic, Z. Asimovic, D. Zavrsnik, DFT study and biological activity of some methylxanthines, Bull. Chem. Technol. Bosnia Herzeg. 42 (2014) 31–36.
[53] Z. Jin, X. Du, Y. Xu, Y. Deng, M. Liu, Y. Zhao, B. Zhang, X. Li, L. Zhang, C. Peng, Y. Duan, J. Yu, L. Wang, K. Yang, F. Liu, R. Jiang, X. Yang, T. You, X. Liu, X. Yang, F. Bai, H. Liu, X. Liu, L.W. Guddat, W. Xu, G. Xiao, C. Qin, Z. Shi, H. Jiang, Z. Rao, H. Yang, Structure of M^{pro} from COVID-19 virus and discovery of its inhibitors, Nature (2020) https://doi.org/10.1038/s41586-020-2223-y.
[54] J.S. Morse, T. Lalonde, S. Xu, W.R. Liu, Learning from the past: possible urgent prevention and treatment options for severe acute respiratory infections caused by 2019-nCoV, Chem. Bio. Chem. 21 (2020) 730–738.
[55] A.K. Patick, K.E. Potts, Protease inhibitors as antiviral agents, Clin. Microbiol. Rev. 11 (1998) 614–627.
[56] P. Calligari, S. Bobone, G. Ricci, A. Bocedi, Molecular investigation of SARS–CoV-2 proteins and their interactions with antiviral drugs, Viruses 12 (2020) 445.
[57] R. Hatada, K. Okuwaki, Y. Mochizuki, K. Fukuzawa, Y. Komeiji, Y. Okiyama, S. Tanaka, Fragment molecular orbital based interaction analyses on COVID-19 main protease - inhibitor N3 complex (PDB ID: 6LU7), ChemRxiv (2020), doi:10.26434/chemrxiv.11988120.v1.